LAWRENCE
LIVERMORE
NATIONAL
LABORATORY

UCRL-JRNL-209759

Synthesis of Yttria-Stabilized Zirconia Aerogels by a Non-Alkoxide Sol-Gel Route

C. N. Chervin, B. J. Clapsaddle, H. W. Chiu, A. E. Gash, J. H. Satcher, Jr., S. M. Kauzlarich

February 16, 2005

Chemistry of Materials

Synthesis of Yttria-Stabilized Zirconia Aerogels by a Non-Alkoxide Sol-Gel Route

Christopher Chervin,[†,‡] Brady J. Clapsaddle,[§] Hsiang Wei Chiu,[†] Alexander E. Gash,[§] Joe H. Satcher Jr.,[§] and Susan M. Kauzlarich[†,]*

[†]Department of Chemistry, University of California at Davis, One Shields Avenue, Davis, CA 95616

[‡]Lawrence Livermore National Laboratory, University Outreach, Livermore, CA 94550

[§]Lawrence Livermore National Laboratory, Chemistry and Materials Science Directorate, Livermore, CA 94550

Abstract

Homogeneous, nanocrystalline powders of yttria-stabilized zirconia were prepared using a non-alkoxide sol-gel method. Monolithic gels, free of precipitation, were prepared by addition of propylene oxide to aqueous solutions of Zr^{4+} and Y^{3+} chlorides at room temperature. The gels

were dried with supercritical $CO_2(l)$, resulting in amorphous aerogels that crystallized into cubic stabilized ZrO_2 following calcination at 500 ^oC. The aerogels and resulting crystalline products were characterized using *in-situ* temperature profile X-ray diffraction, thermal analysis, transmission electron microscopy (TEM), scanning electron microscopy (SEM), and nitrogen adsorption/desorption analysis. TEM and N_2 adsorption/desorption analysis of an aerogel indicated a porous network structure with a high surface area (409 m^2/g). The crystallized yttria-stabilized zirconia maintained high surface area (159 m^2/g) upon formation of homogeneous, nanoparticles (~10 nm). Ionic conductivity at 1000 ^oC of sintered YSZ (1500 ^oC, 3 hours) prepared by this method, was 0.13 ± 0.02 $\Omega^{-1}cm^{-1}$. Activation energies for the conduction processes from 1000 – 550 ^oC and 550 – 400 ^oC, were 0.95 ± 0.09 and 1.12 ± 0.05 eV, respectively. This is the first reported synthesis and characterization of yttria-stabilized zirconia via an aerogel precursor.

Keywords Sol-gel, aerogel, YSZ, zirconia, ZrO_2, epoxide, fuel cell

Introduction

Yttria-stabilized zirconia (YSZ), a high temperature oxide conductor, is a technologically significant material that finds extensive use as a solid-state electrolyte in applications such as solid oxide fuel cells and oxygen sensors.[1] YSZ has also been considered a good candidate for the oxide-conducting component of mixed ionic-electronic conducting composite electrodes.[2] Zirconia, the parent lattice in YSZ, is a polymorphic oxide with a high temperature cubic phase that can be stabilized at room temperature through substitution of Zr^{4+} with rare earth or alkali earth cations.[1] Charge compensation is balanced by the formation of oxygen vacancies which are necessary for thermally activated conduction processes. In the case of Y^{3+} substitution, cubic

stabilization occurs above 7 mol% Y_2O_3.[3] The solid solution range for single phase cubic stabilized ZrO_2 extends to 56 mol% Y_2O_3,[3] with the optimal conductivity occurring near the lower substitution limit.[4] Therefore, most practical electrolyte applications of YSZ use 8 – 10 mol% Y_2O_3.

Particle size and size distribution of precursor powders are important factors to consider when fabricating electrolytes and composite electrodes with YSZ.[5, 6] Homogeneous powders consisting of sub-micrometer particles, free of hard agglomeration, can be beneficial for many fabrication techniques including slip-casting, tape casting, isostatic pressing, and colloidal spray deposition.[7, 8] Nanoparticles have larger surface energies than micron sized particles and as a result, can potentially benefit ceramic processing by lowering sintering temperatures, increasing firing density, and creating nano-sized grains in the fired ceramics.[7, 9, 10] Additionally, recent studies have demonstrated enhanced conductivity in nanocrystalline YSZ and other solid state electrolytes.[8, 11-13] Proposed mechanisms for the increased conductivity include dilution of impurities at the grain boundaries[12-14] and an increased number of defects due to the larger surface to bulk ratio of nanocrystalline materials.[13] Considering the demand for homogeneous, nanocrystalline YSZ powders in both commercial and laboratory applications, simple and effective preparation routes resulting in these morphologies are important and desirable.

Nanocrystalline YSZ has been prepared by various methods including sol-gel synthesis, spray pyrolysis, combustion synthesis, and co-precipitation routes.[15-17] Of these methods, sol-gel synthesis is a very common and exceptional technique because it provides a means of controlling the shape, morphology and textural properties of the final materials.[18] The reported sol-gel techniques for preparing YSZ traditionally utilize alkoxide precursors and organic solvents.[19, 20] These sol-gel techniques are either acid or base catalyzed and require the careful addition of

water to prevent uncontrolled hydrolysis of Zr alkoxides.[18, 21, 22] Furthermore, atmospheric water leads to partial hydrolysis of the precursors, and often the reactions are carried out in nitrogen[23] or dehumidified atmospheres.[24] Chelating agents, such as acetylacetone, are sometimes added to help control hydrolysis during the gelation process.[25] Though these methods are sufficient for preparing nanocrystalline YSZ, simpler methods eliminating the need for alkoxide precursors and thereby the difficulties of handling the water sensitive precursors, would be beneficial.

Recently, Gash and co-workers have reported an alkoxide free, sol-gel synthesis technique for preparing various transition, main group, and rare earth metal oxides.[26-28] Through the use of an organic epoxide that acts as a proton scavenger, solutions of common hydrated metal salts undergo hydrolysis and condensation reactions to form metal oxide sol-gel materials, as shown in Scheme 1.[18, 27, 29, 30] The "epoxide addition method" works well for several metal chloride

Scheme 1. General reaction scheme for the epoxide addition sol-gel process.

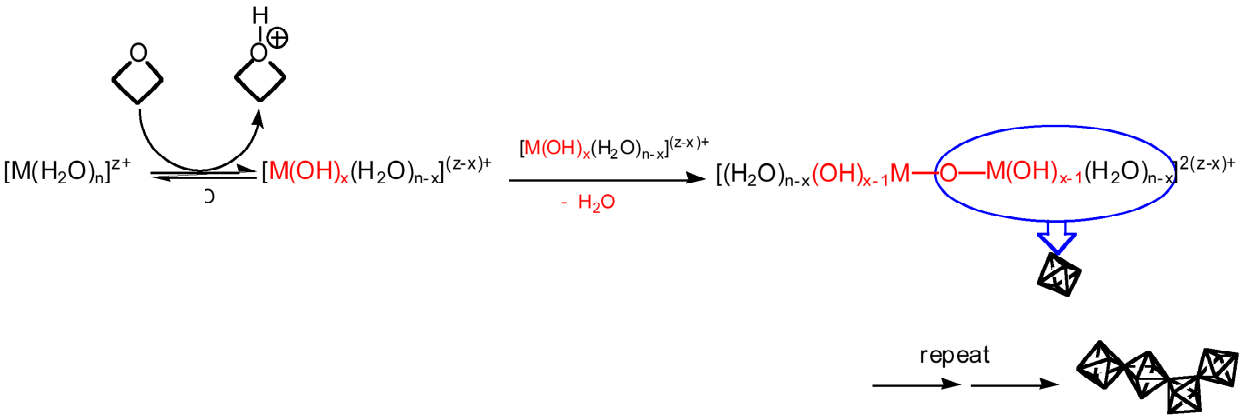

salts in water and other polar protic solvents (provided sufficient water is present), including both Zr^{4+} and Y^{3+} salts. This method eliminates the need for the often difficult preparation and handling of metal alkoxide precursors for non-traditional sol-gel metals and is complimentary to traditionally prepared sol-gel materials (i.e. SiO_2, TiO_2, Al_2O_3, etc.). Some examples of metal oxide gels prepared by the epoxide addition method include Fe_2O_3, Cr_2O_3,

Al_2O_3, Ga_2O_3, and ZrO_2, and the method has also proven useful in the synthesis of a variety of binary metal-oxide systems.[26, 31, 32]

We report here a straightforward synthesis technique for the preparation of YSZ precursor sol-gels using the epoxide addition method. Monolithic gels are easily formed from $ZrCl_4$ and $YCl_3 \cdot 6H_2O$, using propylene oxide in distilled water. The gels are prepared in ambient atmosphere and temperature without elaborate or complicated synthetic equipment. The resultant wet gels are converted to aerogels by supercritical drying in CO_2 or to xerogels by slow drying in ambient atmosphere. Remarkably, the aerogel materials are observed to maintain a nano-structure following heat treatment at temperatures as high as 1000 ˚C, resulting in homogeneous, nanocrystalline powders of YSZ that can be further processed into a variety of forms (e.g. ceramics, thin films, etc). YSZ powders prepared from this technique demonstrated bulk ionic conductivity consistent with literature reported values.

Experimental Section

Synthesis of YSZ Nanoparticles. YSZ-precursor gels containing 9 mol% Y_2O_3 were prepared by the epoxide addition method followed by supercritical drying in $CO_2(l)$. Anhydrous $ZrCl_4$ (99.9+%, Aldrich), $YCl_3 \cdot 6H_2O$ (99.9%, Aldrich), and propylene oxide (99%, Aldrich) were used as received. All gelation reactions were carried out at room temperature in ambient atmosphere. In a typical synthesis, $ZrCl_4$ (1.1652 g; 5 mmol) and $YCl_3 \cdot 6H_2O$ (0.3034; 1 mmol) were dissolved in distilled water (10 g; 555 mmol) such that the molar ratio of water to total metals was 93. Following complete dissolution of the salts, propylene oxide (PO; 3.2 g; 55 mmol) was added and briefly stirred (9:1 epoxide:metals molar ratio) to induce gelation. Clear monolithic gels, free of precipitates, resulted from all reactions.

Following gelation, the gels were aged for 24 hours under ambient conditions in closed containers. The aged gels were then washed with ethanol for three days, with fresh ethanol exchanged daily. Wet gels were processed to aerogels by supercritical drying in a Polaron^{TM} supercritical point drier. Ethanol in the wet gel pores was exchanged for $CO_2(l)$ for 2-3 days, after which the temperature of the vessel was ramped up to ~ 45 ^{o}C, while a pressure of ~ 100 bar was maintained. The vessel was then depressurized at a rate of ~ 7 bar/h. Dried aerogels were calcined in air at 550 and 1000 ^{o}C using 2 ^{o}C /minute ramps and 1 hour dwell times.

Physical Characterization. Thermogravimetric analysis (TGA) and differential scanning calorimetry (DSC) of the resulting aerogels were performed simultaneously with a Netzsch 449 Thermal Analyzer in the temperature range of 25 to 1000 ^{o}C under flowing oxygen using a 10 ^{o}C/minute ramp.

The crystallization of cubic zirconia from the amorphous aerogels was monitored with *in-situ* temperature profile X-ray diffraction using an INEL diffractometer operated at 30 A and 30 keV with Cu K_α radiation. The diffractometer was equipped with a furnace heated sample holder and a position sensitive detector allowing for diffraction measurements at selected temperatures during the calcination process. Diffraction data at each desired temperature was collected for 30 minutes. Room temperature X-ray diffraction patterns of as-prepared and calcined aerogels were measured using a Scintag PAD V diffractometer operating at 40 A and 45 keV with Cu K_α radiation.

Surface area analysis was performed using an ASAP 2000 surface area analyzer (Micromeritics Instrument Corp.). Prior to analysis, samples of approximately 0.1-0.2 g were heated to 200 ^{o}C under vacuum (10^{-5} Torr) for at least 24 h to remove adsorbed species.

Nitrogen adsorption data were taken at five relative pressures from 0.05 to 0.20 at 77 K, and the surface area calculated using BET (Brunauer-Emmett-Teller) theory.

Brightfield transmission electron microscopy (TEM) analyses of an aerogel as prepared and after calcination at 550 and 1000 ^{o}C were performed on a Philips CM-120 TEM, operating at 80 keV. TEM samples were prepared by dipping holey carbon-coated 400-mesh grids into methanol colloids of the respective powders, followed by drying at 120 ^{0}C overnight. Scanning electron microscopy was performed with a Philips 30XL FEG SEM operated between 5 and 10 keV. SEM samples were prepared by applying drops of methanol colloids of the respective powders on to hot aluminum SEM stubs, followed by drying at 120 ^{o}C overnight.

Measurement of d.c. Ionic Conductivity of YSZ. The ionic conductivity as a function of temperature for aerogel derived YSZ powder was measured using the four probe d.c. technique of van der Pauw.[33] YSZ, calcined at 800 ^{o}C, was isostatically pressed into rectangular pellets at 930 bars and then sintered in air at 1500 ^{o}C for 3 hours. YSZ powders were calcined prior to pressing to minimize weight loss during sintering and porosity in the final pellets. Platinum voltage and current electrodes were applied to the sintered pellets as a paste (Heraeus, CL11-5349), and fired at 900 ^{o}C for 30 minutes. The sintered pellets were approximately 1.75 cm in length, 0.1 cm^{2} in cross-section, and the voltage electrode separation was 0.8 cm. Platinum wires were attached to the electrodes with Pt paste followed by an additional sintering at 900 ^{o}C for 30 minutes. The instrument leads were connected to the platinum wires and the samples were placed in quartz tubes.

Conductivity measurements were made in tube furnaces under flowing air (1L/minute) from 1000 – 400 ^{o}C at 50 or 100 ^{o}C intervals, depending on the temperature range. For each temperature a constant current was applied with a Solartron SI 1287 Electrochemical Interface

and the steady-state voltage was measured. Currents ranged from 0.01 A to 1 μA, depending on sample resistivity.

Results and Discussion

Synthesis. Addition of PO to aqueous solutions containing Zr^{4+} and Y^{3+} chlorides resulted in the formation of clear monolithic gels free of precipitates. The gelation time (t_{gel}) was rapid, on the order of minutes, and varied with the molar ratio of PO to total metals, R_{epox}. For a constant volume of water and R_{epox} = 5, 7, and 9, the t_{gel}'s were 4.5, 1.5, and 0.5 minutes, respectively. The t_{gel}'s were qualitatively determined as the point at which the sols no longer flowed under the influence of gravity when the reaction containers were tilted. The gelation points were generally preceded by notable changes in the solution viscosity and a slight degree of opacity.

Supercritical drying of the wet gels resulted in partially monolithic aerogels, which were easily ground into powders. The ultrafine, homogeneous powders had nanoparticulate morphologies, were X-ray amorphous, and upon calcination crystallized into the cubic fluorite structure for stabilized ZrO_2. The variation of R_{epox} during the initial wet-gel synthesis did not appear to have any affect on the final calcined powder morphology or diffraction patterns. For simplicity, the as prepared aerogels will be referred to as YSZ-aerogels but technically speaking they are not cubic stabilized zirconia until after calcination.

Powder X-ray Diffraction. Figure 1 shows *in-situ* temperature profile powder XRD patterns of a YSZ aerogel prepared with R_{epox} = 9. The diffraction patterns were measured immediately after reaching the desired temperature and once again after dwelling at the specific temperature for 1.5 hours. The YSZ-aerogel was X-ray amorphous up to 450 ^{o}C. Crystallization had partially occurred by 500 ^{o}C and crystallinity increased with prolonged calcination at that temperature. Further calcination to 550 ^{o}C did not significantly alter the diffraction pattern.

Room temperature XRD of the sample following heat treatment at 550 ^{o}C is shown in Figure 2. The peak positions are in agreement with the reported reflections for cubic zirconia (PDF Card # 82-1246). The significant amount of peak broadening observed is due to the nanocrystalline nature of the calcined aerogel.

Thermal Analysis. Figure 3 shows the simultaneous TGA/DSC traces for an aerogel prepared with R_{epox} = 9. Several major peaks are observed in the DSC curve and each corresponds to weight loss measured by TGA. The first peak is a broad endotherm with a minimum at 139 ^{o}C that is attributed to the combined loss of water and residual organics from the gel preparation. This peak occurs concurrently with a TGA weight loss of 16.33%. The second DSC peak, a sharp exotherm with a maximum at 235 ^{o}C, is likely due to oxidation of residual organic compounds and corresponds to a sharp weight loss of 3.37%. Two additional exotherms occur with maxima at 309 and 405 ^{o}C and a combined weight loss of 13.10%. The total mass loss for the gel heated to 1000 ^{o}C, as determined by TGA, was 36.12%, the majority of which occurred below 400 ^{o}C (30.04%). The remaining 6.08% weight loss above 400 ^{o}C is likely due to elimination of water as chemisorbed hydroxyl groups react to form additional M-O-M bonds.[34]

A distinct exotherm related to crystallization was not observed in the DSC data, however, a small, broad exothermic feature is discernable from 450-500 ^{o}C. Based on XRD results (Figures 1 and 2), the crystallization of YSZ was expected to occur above 450 ^{o}C with the phase transition only partially occurring upon reaching 500 ^{o}C. Prolonged calcination at that temperature was required to complete formation of a highly nanocrystalline cubic phase. Considering the DSC heating rate of 10 ^{o}C/min, it is not unexpected to find a broad exotherm as opposed to a sharp crystallization peak. The observed three exotherms at temperatures below 450 ^{o}C correspond closely with sharp weight losses and amorphous XRD structures, and therefore are attributed to

the oxidation of residual organic components or formation of M-O-M bonds through condensation and elimination of H_2O.

Electron Microscopy. Brightfield TEM images confirm that the YSZ-aerogels crystallize into powders that remain nano-particulate even after high temperature calcination. Micrographs of a YSZ-aerogel and samples calcined at 550 and 1000 ^oC are shown in Figure 4. An extended nano-particulate network resulted during the sol-gel processing of the YSZ-aerogel (Figure 4a). Following calcination at 550 ^oC, individual YSZ particles are distinguishable with diameters under 10 nm (Figure 4b). After calcination at 1000 ^oC, particle sizes increased to 30-40 nm, but without any further change in morphology (Figure 4c). These results indicate that the extended network of the original YSZ-aerogel is no longer present after calcination, but instead crystalline powders of nanometer sized particles with narrow size distributions are obtained. SEM images of the powder calcined at 550 and 1000 ^oC, shown in Figure 5, further confirm the homogeneous, nanoscopic nature of the YSZ. In addition, SEM analysis reveals no evidence of hard agglomeration in the final powders.

Surface Area Analysis. The surface area of the porous networked YSZ-aerogel (Figure 4a) was 406 m^2/g. Following calcination at 550 and 1000 ^oC, the YSZ surface areas were 159 and 26.0 m^2/g, respectively. Using the experimentally determined surface areas and assuming all particles are spherical, the average particle size (d_{BET}) can be calculated for the powders using

$$d_{BET} = 6/(\rho S_v), \quad (1)$$

where ρ is the materials density and S_v the specific surface area of the sample. Using the theoretical density of 5.9503 g/cm^3 for 9 mol% Y_2O_3-stabilized ZrO_2,[35] the calculated d_{BET} for

the aerogels calcined at 550 and 1000 ^{o}C were 6.3 and 39 nm, respectively, in good agreement with the TEM data. The average particle size for the YSZ-aerogel was not calculated because the density of the amorphous oxide is unknown. In addition, the TEM data indicate that the amorphous particles exist in extended porous networks and are not spherical in nature.

Gel Structure. In this study gelation occurred in a homogeneous fashion from the precursor solution, which suggests the extended network that formed contained uniformly mixed Y^{3+} and Zr^{4+} oxo-species.[29] The actual composition of the YSZ-aerogel is unknown, but certainly contains a high degree of hydroxyl groups, as is evidence from the significant weight loss during calcination. Uniform mixing of Y^{3+} and Zr^{4+} is apparent by *in-situ* XRD data, revealing crystallization of cubic Y_2O_3-stabilized ZrO_2 at low temperature without intermediate oxide formation. In the absence of dopants, ZrO_2 crystallizes into a monoclinic structure.[3] Furthermore, TEM and SEM demonstrate the oxide is extremely homogeneous with no evidence of phase separation. Extended binary oxide networks that were formed during the sol-gel process are inherently mixed on the atomic level, which is a key advantage over conventional solid state synthesis techniques.

The monolithic sol-gels were sensitive to the drying step and resulted in significantly different morphologies depending on the drying method. Supercritical drying (aerogels) produced fluffy, soft materials, whereas drying under ambient conditions (xerogels) resulted in very coarse materials that were difficult to grind to fine powder. Furthermore, when using xerogel starting materials, hard agglomerates were obtained upon calcination as opposed to the distinct nano-particles obtained from the aerogel starting materials. The difference in morphology, crystallinity, surface area, and particle agglomeration between xerogel and aerogel processed gels are currently under investigation.

Ionic Conductivity. Electrical resistivity of YSZ is measured as a function of temperature and in general reported as conductivity (σ)

$$\sigma = 1/R, \quad (2)$$

where R is the bulk resistivity of the material. The temperature dependence of YSZ can be expressed as:

$$\sigma(T) = A/T\exp(-E_a/kt), \quad (3)$$

where E_a is the activation energy, k is the Boltzmann constant, and A is the pre-exponential factor.[36] The activation energy for the conduction process is obtained from the slope of a plot of ln (σT) versus 1/T.

Figure 6 shows ln (σT) as a function of 10^4/T plotted for 3 sintered YSZ pellets prepared from calcined aerogel powders. The geometric density of the pellets, which are labeled A1, A2, and A3 were 95.2, 94.9, and 96.8% of theoretical,[35] respectively. The data show a change in slope around 550 ^{o}C towards lower activation energy at higher temperature, in agreement with previously reported results for YSZ.[37, 38] The activation energies, determined separately for the two temperature regions of 400 – 550 ^{o}C and 550 – 1000 ^{o}C, are listed in Table 1. Also listed in Table 1 are the bulk ionic conductivities for each sample at 1000 and 800 ^{o}C, both common operating temperatures for solid oxide fuel cells utilizing YSZ components.

The ionic conductivities for the sintered YSZ aerogel at 800 and 1000 ^{o}C were 0.036 ± .005 and 0.13 ± 0.02 Ω^{-1}cm^{-1}, respectively. These are in good agreement with accepted values for

total conductivity of 9 mol% YSZ at the respective temperatures.[1, 39] The activation energies for the high and low temperature regions were 0.95 ± 0.09 and 1.12 ± 0.05 eV, respectively. These results, within experimental error, are in agreement with work by Petot et al. for the activation energies in single crystal 9 mol% YSZ, which were found to be 0.93 ± 0.03 and 1.08 ± 0.03 for the high and low temperature regions, respectively.[37]

The 4-probe, d.c. method is used to obtain total resistivity, which for YSZ is composed of bulk and grain boundary contributions.[38] In this study we have measured total resistivity of YSZ sintered at high temperature (1500 ^{o}C) to demonstrate the materials suitability as an oxide conductor for electrolyte and composite cathode applications. We are currently investigating the effects of these high surface area, nanocrystalline YSZ in SOFC composite cathode applications. Potentially, aerogel derived YSZ will provide reduced sintering temperature, larger surface area, and improved reaction kinetics of the porous cathodes.

Conclusions

The epoxide addition sol-gel method was successfully applied to the synthesis of yttria-stabilized zirconia. This technique provides a straightforward method for the preparation of homogeneous YSZ precursor gels in aqueous solution without the need for alkoxide precursors or elaborate reaction schemes. Supercritical drying of the wet gels produced ultrafine, homogeneous powders with nano-particulate morphologies. The amorphous, aerogels crystallized into the cubic phase of YSZ at approximately 500 ^{o}C while maintaining a high surface area and particle diameters below 10 nm. Conductivity measurements of sintered YSZ aerogels were in excellent agreement with previous reported data for YSZ. The materials prepared by this method are currently being evaluated for potential use in solid oxide fuel cell composite cathodes.

Acknowledgements

This work was supported by the University of California Energy Institute, the National Science Foundation (Grant DMR-0120990), and the Department of Energy (Student Employee Graduate Research Fellowship). The authors thank Alexandra Navrotsky, for use of the Scintag X-ray diffractometer and TGA/DSC, and David W. Sprehn for technical support. This work was performed under the auspices of the US Department of Energy by the University of California, Lawrence Livermore National Laboratory under contract No. W-7405-Eng-48.

References

(1) Subbarao, E. C.; Maiti, H. S. *Solid State Ionics* **1984,** 11, (4), 317-38.
(2) Minh, N. Q. *Journal of the American Ceramic Society* **1993,** 76, (3), 563-88.
(3) Duwez, P.; Brown, F. H., Jr.; Odell, F. *Journal of the Electrochemical Society* **1951,** 98, 356-62.
(4) Dixon, J. M.; LaGrange, L. D.; Merten, U.; Miller, C. F.; Porter, J. T. *Journal of the Electrochemical Society* **1963,** 110, 276-80.
(5) Sasaki, K.; Wurth, J. P.; Gschwend, R.; Godickemeier, M.; Gauckler, L. J. *Journal Of The Electrochemical Society* **1996,** 143, (2), 530-543.
(6) Kim, J. D.; Kim, G. D.; Moon, J. W.; Lee, H. W.; Lee, K. T.; Kim, C. E. *Solid State Ionics* **2000,** 133, (1-2), 67-77.
(7) Mistler, R. E.; Twiname, E. R., *Tape casting: theory and practice*. Amercian Ceramic Society: Westerville, OH, **2000**.
(8) Xu, G.; Zhang, Y.-W.; Liao, C.-S.; Yan, C.-H. *Solid State Ionics* **2004,** 166, (3-4), 391-396.
(9) McColm, I. J., In *Ceramic Processing*, ed.; R.A. Terpstra, P. P. A. C. P., and De Vries, Chapman and Hall: New York, **1995**; pp 17-18.
(10) King, A. G., *Ceramic Technology and Processing*. William Andrew Publishing: New York, **2002**.
(11) Mondal, P.; Klein, A.; Jaegermann, W.; Hahn, H. *Solid State Ionics* **1999,** 118, (3,4), 331-339.
(12) Kosacki, I.; Anderson, H. U. *Ionics* **2000,** 6, (3 & 4), 294-311.
(13) Tuller, H. L. *Solid State Ionics* **2000,** 131, (1,2), 143-157.
(14) Kharton, V. V.; Marques, F. M. B. *Current Opinion in Solid State & Materials Science* **2002,** 6, (3), 261-269.

(15) Ramamoorthy, R.; Sundararaman, D.; Ramasamy, S. *Solid State Ionics* **1999,** 123, (1-4), 271-278.
(16) Jiang, S.; Schulze, W. A.; Amarakoon, V. R. W.; Stangle, G. C. *Journal of Materials Research* **1997,** 12, (9), 2374-2380.
(17) Gaudon, M.; Djurado, E.; Menzler, N. H. *Ceramics International* **2004,** 30, (8), 2295-2303.
(18) Brinker, C. J.; Scherer, G. W., *Sol-Gel Science*. ed.; Academic Press: Boston, 1990; 'Vol.' p.
(19) Okubo, T.; Nagamoto, H. *Journal of Materials Science* **1995,** 30, (3), 749-57.
(20) Ayral, A.; Assih, T.; Abenoza, M.; Phalippou, J.; Lecomte, A.; Dauger, A. *Journal of Materials Science* **1990,** 25, (2B), 1268-74.
(21) Wolf, C.; Ruessel, C. *Journal of Materials Science* **1992,** 27, (14), 3749-55.
(22) Shukla, S.; Seal, S.; Vij, R.; Bandyopadhyay, S. *Nano Letters* **2003,** 3, (3), 397-401.
(23) Okubo, T.; Takahashi, T.; Sadakata, M.; Nagamoto, H. *Journal of Membrane Science* **1996,** 118, (2), 151-157.
(24) Xia, C.; Cao, H.; Wang, H.; Yang, P.; Meng, G.; Peng, D. *Journal of Membrane Science* **1999,** 162, (1-2), 181-188.
(25) Debsikdar, J. C. *Journal of Non-Crystalline Solids* **1986,** 86, (1-2), 231-40.
(26) Gash, A. E.; Tillotson, T. M.; Satcher, J. H., Jr.; Hrubesh, L. W.; Simpson, R. L. *Journal of Non-Crystalline Solids* **2001,** 285, (1-3), 22-28.
(27) Gash, A. E.; Tillotson, T. M.; Satcher, J. H., Jr.; Poco, J. F.; Hrubesh, L. W.; Simpson, R. L. *Chemistry of Materials* **2001,** 13, (3), 999-1007.
(28) Gash, A. E.; Satcher, J. H., Jr.; Simpson, R. L. *Chemistry of Materials* **2003,** 15, (17), 3268-3275.
(29) Livage, J.; Henry, M.; Sanchez, C. *Progress in Solid State Chemistry* **1988,** 18, (4), 259-341.
(30) Cotton, F. A.; Wilkinson, G., *Advanced Inorganic Chemistry*. 5th ed.; John Wiley and Sons: New York, 1988; 'Vol.' p.
(31) Clapsaddle, B. J.; Gash, A. E.; Satcher, J. H.; Simpson, R. L. *Journal of Non-Crystalline Solids* **2003,** 331, (1-3), 190-201.
(32) Clapsaddle, B. J. S., D. W.; Gash, A. E.; Satcher, J. H. Jr.; Simpson, R. L., *Journal of Non-Crystalline Solids* **2004,** in press.
(33) Van der Pauw, L. J., *Philips Research Reports* **1958,** 13, 1-9.
(34) Hench, L. L.; West, J. K. *Chemical Reviews (Washington, DC, United States)* **1990,** 90, (1), 33-72.
(35) Ingel, R. P.; Lewis, D., III. *Journal of the American Ceramic Society* **1986,** 69, (4), 325-32.
(36) Strickler, D. W.; Carlson, W. G. *Journal of the American Ceramic Society* **1965,** 48, (6), 286-9.
(37) Petot, C.; Filal, M.; Rizea, A. D.; Westmacott, K. H.; Laval, J. Y.; Lacour, C.; Ollitrault, R. *Journal of the European Ceramic Society* **1998,** 18, (10), 1419-1428.
(38) Badwal, S. P. S. *Journal of Materials Science* **1984,** 19, (6), 1767-76.
(39) Etsell, T. H.; Flengas, S. N. *Chemical Reviews (Washington, DC, United States)* **1970,** 70, (3), 339-76.

Table 1. Activation energy and conductivity results for sintered YSZ aerogels.

Sample	E_a > 550 ^oC (eV)	E_a < 550 ^oC (eV)	σ at 800 ^oC ($\Omega^{-1}cm^{-1}$)	σ at 1000 ^oC ($\Omega^{-1}cm^{-1}$)
A1	0.96 ± 0.06	1.12 ± 0.03	0.032 ± 0.004	0.12 ± 0.02
A2	0.95 ± 0.06	1.13 ± 0.03	0.039 ± 0.001	0.140 ± 0.004
A3	0.94 ± 0.06	1.10 ± 0.03	0.036 ± 0.002	0.130 ± 0.006

Figure Captions

Figure 1. *In-situ* temperature profile XRD of a YSZ aerogel. Diffraction patterns were measured immediately after reaching each temperature and once again after dwelling for 1.5 hours. Only selected diffraction profiles are shown to prevent redundancy. Additional peaks associated with the Al_2O_3 sample holder become apparent during shrinkage of the sample during heating. The sharp Al_2O_3 peaks are easily distinguished from the broad (nanocrystalline) YSZ phase and are marked with an *.

Figure 2. Room temperature XRD pattern of an YSZ aerogel calcined at 550 ^oC. Peak positions from PDF Card # 82-1246 (cubic yttria-stabilized ZrO_2) are marked with sharp lines.

Figure 3. Simultaneous TGA/DSC scans of a dried YSZ aerogel, R_{epox} = 9, (10 ^oC/minute ramp under flowing oxygen).

Figure 4. Brightfield TEM micrographs of a YSZ aerogel, $R_{epoxide}$ = 9, (a) as-prepared (b) calcined at 550 ^{o}C and (c) calcined at 1000 ^{o}C.

Figure 5. SEM images of a YSZ aerogel calcined at (a) 550 ^{o}C and (b) 1000 ^{o}C.

Figure 6. Plot of ln (σT) as a function of 10^4/T for sintered YSZ pellets prepared from aerogel powders.

Figure 1

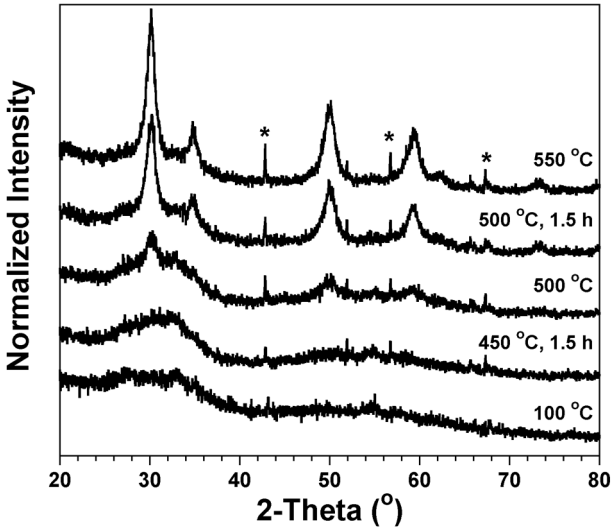
Normalized Intensity
2-Theta (°)
20
30
40
50
60
70
80
*
*
*
550 °C
500 °C, 1.5 h
500 °C
450 °C, 1.5 h
100 °C

Figure 2

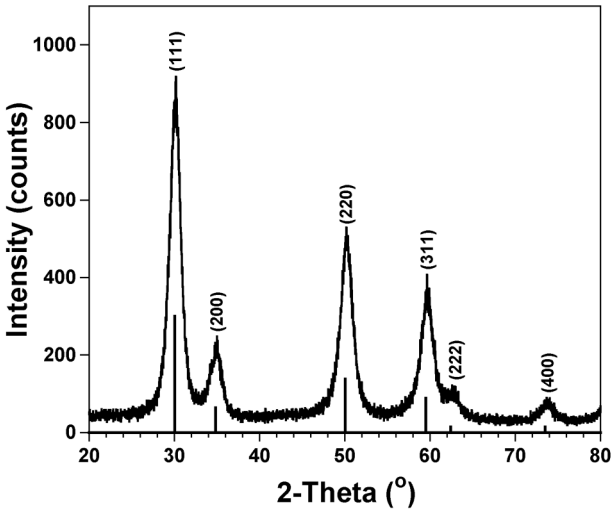
Intensity (counts)
2-Theta (°)
(111)
(200)
(220)
(311)
(222)
(400)
0
200
400
600
800
1000
20
30
40
50
60
70
80

Figure 3

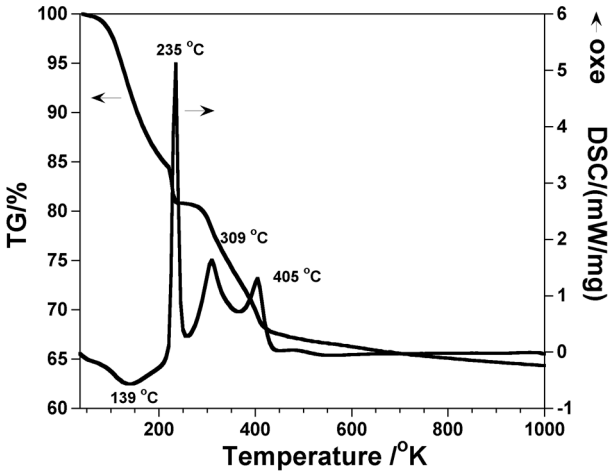
TG/%
DSC/(mW/mg)
↑ exe
Temperature /°K
235 °C
309 °C
405 °C
139 °C
100
95
90
85
80
75
70
65
60
6
5
4
3
2
1
0
-1
200
400
600
800
1000

Figure 4a

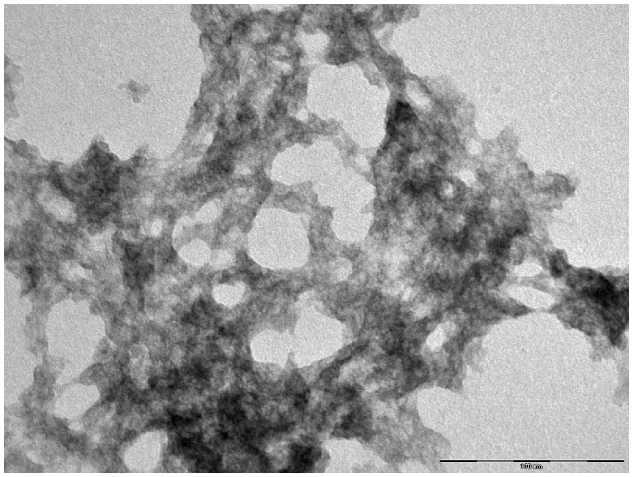

Figure 4b

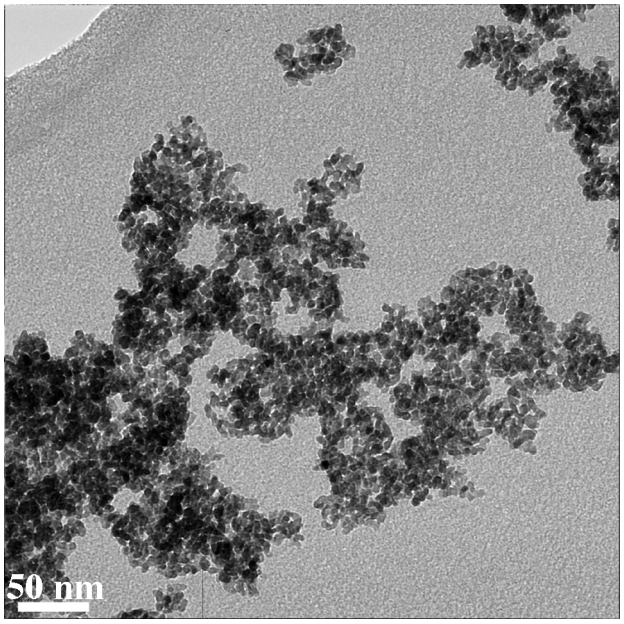

Figure 4c

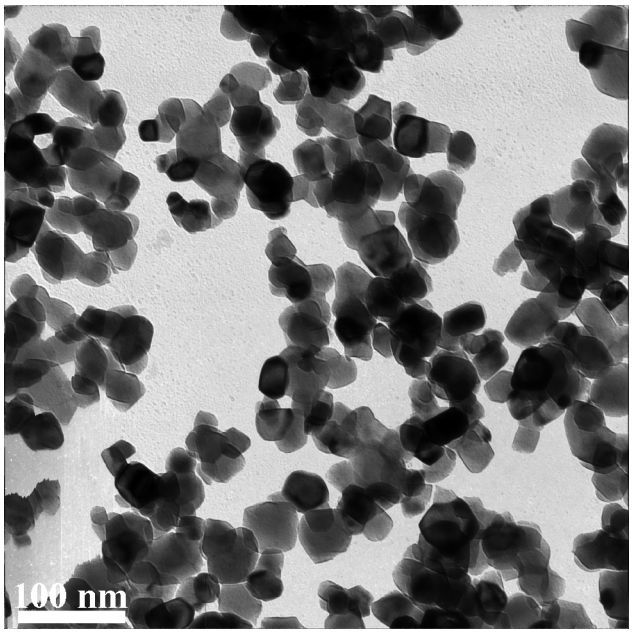

Figure 5a

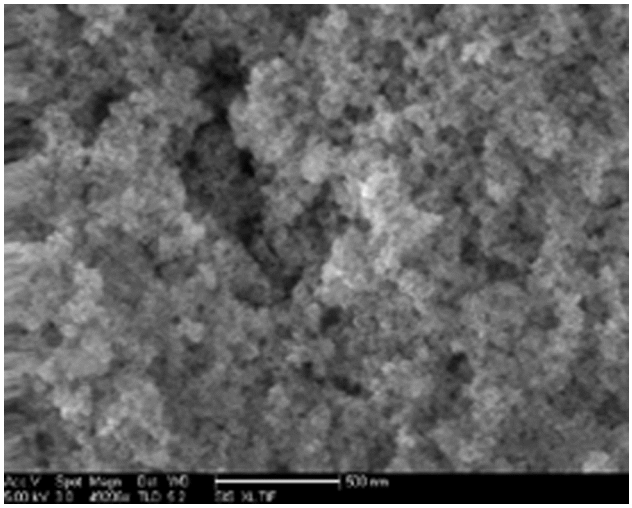

Figure 5b

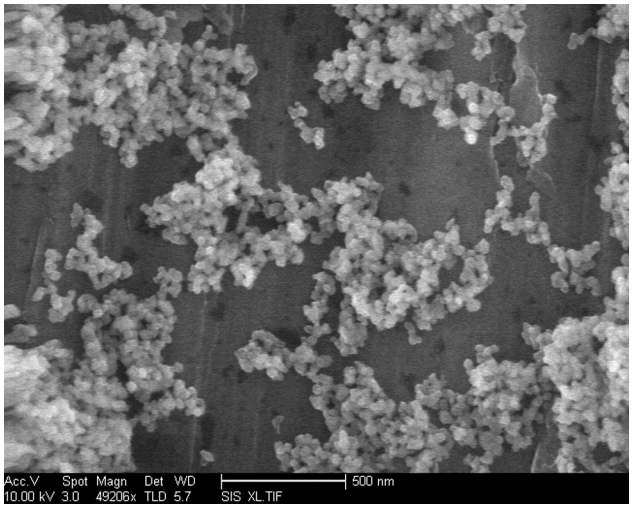

Figure 6